KSME

Springer

Journal of Mechanical Science and Technology 35 (4) 2021

Original Article
DOI 10.1007/s12206-021-0317-6

Keywords:
· Bubble dispersion
· Turbulence modification
· Two-way interaction
· Immersed boundary method

Correspondence to:
Hyoeun Shim
hyoeun92@yonsei.ac.kr;
Changhoon Lee
Clee@yonsei.ac.kr

Citation:
Shim, H., Lee, C. (2021). Two-way interaction between isotropic turbulence and dispersed bubbles. Journal of Mechanical Science and Technology 35 (4) (2021) 1527~1537.
http://doi.org/10.1007/s12206-021-0317-6

Received September 30th, 2020
Revised November 24th, 2020
Accepted December 14th, 2020

† Recommended by Editor
Yang Na

Two-way interaction between isotropic turbulence and dispersed bubbles

Hyoeun Shim and Changhoon Lee

Department of Computational Science and Engineering, Yonsei University, 134 Shinchon-dong, Seodaemun-gu, Seoul 120-749, Korea

Abstract Two-way interaction-mediated modification of isotropic turbulence and bubble dispersion is investigated using direct numerical simulations. The asymmetric coupling force on vortical structures generates horizontal force gradients, transiently enhancing the flow vorticity, while the cumulative buoyant transfer induced by bubbles in the downflow regions decreases it by attenuating the horizontal gradients of the downward flow velocity. These vorticity fluctuations affect the non-uniform distortion in the flow dissipation spectrum with a large-scale energy reduction, decreasing the flow dissipation. In addition, the buoyancy force acting on the bubbles affects the bubble distribution. Smaller inhomogeneities in the bubble distribution with turbulence attenuation, owing to the two-way coupling effects, also contribute to the bubble dispersion.

1. Introduction

Bubble-laden turbulent flows are observed in many natural and technological settings. Examples include oceanographic phenomena (i.e., transfer of carbon dioxide on the surface of the ocean [1]) and chemical engineering processes (i.e., bubble columns [2]). These observations have necessitated the need for better understanding of both the spatial distributions of bubbles and the macroscopic effect on turbulence caused by the bubble phase.

Experimental measurements, together with numerical simulations of one-way coupling where the momentum transfer from bubbles to the carrier flow is not considered, have focused on how the bubbles behave within the carrier turbulence. The behavior characteristics of bubbles that are different from those in still fluids, namely preferential bubble clustering in the cores of vortical structures and reduction of the mean bubble rising velocity in turbulence, have been of interest [3, 4]. Aliseda and Lasheras [3] experimentally measured the behaviors of small, spherical, air bubbles in homogeneous isotropic turbulence. They confirmed a reduction in the bubble rising velocity compared with the quiescent fluid, which turned out to be maximal for bubbles with the Stokes number (τ_b / τ_η ; τ_b = bubble response time, τ_η = Kolmogorov time scale of turbulence) on the order of unity. They also experimentally demonstrated inhomogeneities in the bubbles' spatial distributions induced by the dynamics of the carrier turbulence. Mazzitelli and Lohse [4] numerically examined prominent clustering in isotropic turbulence. They found that the preferential concentration ofbubbles in the cores of vortical structures was maximized when the bubble rising velocity and the bubble response time were equal to the Kolmogorov velocity and time scales, respectively.

On the other hand, for two-way coupling where the backreaction of bubbles with respect to the carrier flow is considered, numerical simulations have shown that bubbles drive different responses of the carrier turbulence in terms of the length scales related to the interphase momentum exchange, which in turn yields non-uniform turbulence modification [5-7]. Mazzitelli et al. [5] numerically examined the turbulence modulation by non-deformable, surfactant-free microbubbles for a Taylor-scale Reynolds number Re_λ = 62. They found that bubbles incited the flow in their surroundings, whereas the energy contained in large-scale structures was attenuated owing to the buoyant transfer from the bubbles in the downflow regions of the

structures, leading to a net decrease in the turbulent kinetic energy. They also demonstrated that the inviscid expression of the lift coefficient was appropriate not only for describing the motion of microbubbles with zero-shear stress boundary conditions where the force balance for this bubble regime had been discussed extensively in previous studies, but also to explain the observed large-scale energy reduction [8, 9]. Van den Berg et al. [7] experimentally confirmed non-uniform energy distortion by microbubbles in fully developed turbulence.

While studies concerning the bubble dispersion and bubble-induced turbulence modification have extended the overall understanding of interactions between the two phases, the dispersion pattern of bubbles within the carrier turbulence under the action of two-way coupling has not been fully addressed. Although it is still unclear whether the spatial distributions of bubbles are considerably influenced by the dynamics of the carrier flow under interphase coupling, previous numerical simulations have suggested that two-way coupling can significantly alter the global quantities of the carrier flow. This in turn implies that the bubble dispersion is inextricably linked to two-way interactions [6, 10]. However, in contrast to the well-studied problem of solid particle-laden turbulent flows [11-15], very few studies have provided the velocity and spatial distributions of bubbles in the context of two-way coupling. For instance, most numerical simulations that incorporate two-way coupling have focused on examining how the global properties of the flow are modified, and attempt to clarify the origin of the observed non-uniform distortion. Some studies have addressed both the issues of the flow modification and the characteristics of the bubble dispersion under two-way coupling, but in slightly different contexts (i.e., the existence of a stable point near the core of a vortical structure) [6], or for different bubble regimes (i.e., no slip boundary conditions at the bubble surface) [10]. Therefore, the motivation of the present study was to investigate the bubble dispersion in homogeneous and isotropic turbulence, under two-way coupling. Bubble Lagrangian velocity autocorrelation functions, bubble diffusivity, and pair dispersion were examined, together with those obtained in simulations that incorporate one-way coupling, to quantitatively describe the dispersion pattern of bubbles that is expected to be different from the one obtained for one-way coupling.

The paper is organized as follows. In Sec. 2 the overall numerical approach is described. In Sec. 3 we examine the effects of two-way coupling on the fluid vorticity, fluid dissipation spectrum, and several global quantities of the fluid. Then, the statistics of the bubble dispersion are presented and compared with those for the case of one-way coupling.

2. Numerical methods

2.1 Flow simulation

The continuity equation and the Navier–Stokes equation for an incompressible flow read

Table 1. Flow parameters.

N	ν	Re_λ	$\langle u'^2\rangle^{1/2}$	ε	l
128	0.018	62.1	2.54	8.89	1.01

η	λ	$k_{\max}\eta$	τ_η	τ_0	v_η
0.028	0.44	1.68	0.0441	1.09	0.63889

$$\frac{\partial u_i}{\partial x_i} = 0, \tag{1}$$

$$\frac{\partial u_i}{\partial t} + \frac{\partial (u_i u_j)}{\partial x_j} = -\frac{\partial p}{\partial x_i} + \nu \frac{\partial^2 u_i}{\partial x_j \partial x_j} + F_i + f_{b,i} \tag{2}$$

where p is pressure, F_i is an artificial forcing for maintaining statistically stationary turbulence, and $f_{b,i}$ is the coupling force between the two phases. The computational domain is a cube of side 2π, subjected to periodic boundary conditions with 128^3 grid points. Eq. (2) is discretized spatially in the wavenumber space, employing the spectral numerical method. Nonlinear terms are calculated in the physical space and viscosity terms are integrated exactly with an exponential function. The resulting equations are solved in time by applying an explicit third-order Runge–Kutta scheme. In addition, the artificial forcing scheme suggested by Eswaran and Pope [16] is applied to maintain stationary turbulence.

Some fundamental properties of the flow field are tabulated in Table 1. These properties are accumulated for ~3 eddy turnover times $3\tau_0$, with $\tau_0 = 3/2\langle u'^2\rangle/\varepsilon$. In Table 1, L denotes the integral length scale, η is the Kolmogorov length scale, λ is the Taylor micro-scale. These length scales are defined as

$$L = \frac{\pi}{2u'^2}\int_0^{k_{\max}} k^{-1}E(k)dk, \tag{3}$$

$$\eta = (\nu^3/\varepsilon)^{1/4}, \tag{4}$$

$$\lambda = (15\nu\langle u'^2\rangle/\varepsilon)^{1/2}, \tag{5}$$

where $E(k)$ is the energy spectrum, ε is the dissipation rate, and $\langle u'^2\rangle^{1/2}$ is the root mean square velocity fluctuation. The other parameters are the Kolmogorov time scale τ_η, the Kolmogorov velocity scale v_η, and $k_{\max} = \sqrt{2}N/3$ is the maximal wave number used in these simulations. Here, $N = 128$ denotes the number of the grid points in each direction. The value of $k_{\max}\eta$ is 1.69 in the present simulations, ensuring correct resolution for small-scale statistics [16]. In addition, the Courant number in the present simulations is 0.03 for obtaining accurate temporal solutions [17]. The Reynolds number is based on the Taylor micro-scale and is defined as

$$\mathrm{Re}_\lambda = \lambda(\langle u'^2\rangle)^{1/2}/\nu. \tag{6}$$

2.2 Bubble simulation

In the present work, we focus on non-deformable microbubbles with radius a that is smaller than the smallest length scale of the flow. The relevant equation of motion for the bubbles is

$$\rho_b V_b \frac{dv_i}{dt} = (\rho_b - \rho_f)V_b g - C_D \frac{\pi a^2}{2}\rho_f |v_i - u_i|(v_i - u_i) + \rho_f V_b C_M (\frac{Du_i}{Dt} - \frac{dv_i}{dt}) + \rho_f V_b \frac{Du_i}{Dt} - C_L \rho_f V_b (v_i - u_i)\times\omega_i, \quad (7)$$

where ρ_f is the density of the fluid, ρ_b is the density of a bubble, V_b is the volume of a bubble, v_i is the bubble velocity, u_i is the fluid velocity evaluated at the location of the bubble, and ω_i is the fluid vorticity [18]. The terms on the right hand side of Eq. (7) represent the buoyancy, the drag, the added mass, the fluid acceleration, and the lift force, respectively. The reader is referred to Refs. [4, 5, 8, 9, 19, 22, 23] for a detailed discussion about these terms. C_M, C_D, and C_L are the added mass, the drag, and the lift force coefficients, and for bubble Reynolds number order of one, the value of each coefficient is taken as 1/2, 16/Re, 1/2, respectively [4, 5, 18]. Then the following equation of motion can be eventually obtained:

$$\frac{dv_i}{dt} = 3\frac{Du_i}{Dt} - \frac{1}{\tau_b}(v_i - u_i) - 2g - (v_i - u_i)\times\omega_i, \quad (8)$$

which will govern the motion of the bubbles for the present simulations. Here, τ_b is the bubble response time, and for the bubble Reynolds number $\mathrm{Re}_b = 2|u_i - v_i|a/\nu$ smaller than unity ($\mathrm{Re}_b < 1$), the bubble response time is given by $\tau_b = a^2/6\nu$ and the corresponding bubble rising velocity in a quiescent fluid is $v_T = 2g\tau_b$ [20, 21]. In addition, bubbles are treated as point spheres and the four-point Hermite interpolation is employed for obtaining the fluid velocity at the bubble, and the bubble velocity is time-advanced using the third-order Runge–Kutta scheme [24].

2.3 Point-force approximation

As shown by Saffman [25], fluid disturbance owing to a particle decreases as the sum of two terms, namely long-range interactions and short-range interactions, which scale as $1/r$ and $(1/r)^3$, respectively. In the present context of Eq. (8) (i.e., for a dilute dispersed phase of bubbles with radii smaller than the smallest length scale of the flow) contribution from the short-range term is negligible because disturbances in this range are sufficiently small and can be dissipated by the fluid viscosity. Therefore, the fluid's Navier-Stokes equations can be written as Eq. (2), where the backreaction of bubble *n* on the fluid can be taken into account by applying Dirac distributions of the force f_b^n to the fluid [26]. Here, f_b^n is the opposite of the force exerted on each bubble *n* by the fluid and can be related to the coupling force $f_{b,i}$ shown in Eq. (2) as follows:

$$f_{b,i} = f_b^n \delta(x_i - X_i^n(t)), \quad (9)$$

where $X^n(t)$ denotes the instantaneous position of bubble *n*.

As shown by Maxey et al. [27], the force specification relies on the specific conditions of the considered fluid. In the present bubble regime we consider bubbles with radii much smaller than the smallest length scale of the fluid, or with the bubble Reynolds number $\mathrm{Re}_b < 1$. f_b^n thus includes forces that arise owing to the relative motion of bubbles in the fluid, and thus can be evaluated using the drag, the added mass, and the lift force, which are the opposite to those exerted on bubble *n* by the fluid:

$$\rho_f f_b^n = \frac{\rho_f V_b}{2\tau_b}(v_i - u_i) - \rho_f V_b \frac{1}{2}(\frac{Du_i}{Dt} - \frac{dv_i}{dt}) + \frac{1}{2}\rho_f V_b((v_i - u_i)\times\omega_i). \quad (10)$$

The contribution of the added mass term to the f_b^n can be evaluated from Eq. (8) as

$$\rho_f V_b \frac{1}{2}(\frac{Du_i}{Dt} - \frac{dv_i}{dt}) = \rho_f V_b (\frac{1}{2\tau_b}(v_i - u_i) - \frac{Du_i}{Dt} + g + \frac{1}{2}(v_i - u_i)\times\omega_i) \quad (11)$$

finally yielding

$$f_b^n = V_b(\frac{Du_i}{Dt} - g). \quad (12)$$

To implement the coupling force f_b^n at Eulerian locations, the class of discrete delta functions introduced by Peskin [28] is used, which was originally formulated for predicting the flows in the human heart. The central idea behind this strategy is that in the context of the Eulerian-Lagrangian approach for two-phase flows where two-way interactions are considered via a singular force, our point bubbles can be thought of as a set of Lagrangian points used for describing the surfaces of immersed bodies. However, unlike the latter case, in which the boundary points move with the local fluid velocity, the present bubbles follow their own equation of motion [29]. This approach, which utilizes discrete delta functions, enables a smoother transfer of the coupling force than the linear interpolation approach, significantly improving the accuracy of the force transfer [30, 31]. The three-dimensional discrete delta function used here for transferring the coupling force to the Eulerian grid points takes the following form [30]:

$$\delta_h(x_i) = d_h(x_1)d_h(x_2)d_h(x_3), \quad (13)$$

where

$$d_h(r) = \begin{cases} \frac{1}{8h}(3-2|r|/h+\sqrt{1+4|r|/h-4(|r|/h)^2}, & |r|\le h, \\ \frac{1}{8h}(5-2|r|/h-\sqrt{-7+12|r|/h-4(|r|/h)^2}), & h\le|r|\le 2h, \\ 0, & otherwise, \end{cases} \quad (14)$$

and h denotes the mesh size.

Then, the coupling force $f_{b,i}$ that is incorporated into the fluid momentum equations is calculated according to

$$f_{b,i}^{N(x,y,z)} = \sum f_b^n \delta_h(x_i - X_i^n(t)), \quad (15)$$

where $N(x,y,z)$ indicates a node surrounded by each bubble *n*.

3. Results

Bubbles are released randomly throughout the entire domain with an initial velocity equal to that of the local fluid; simulations are advanced for ~3 eddy turnover times, to achieve a statistically stationary state. Then, the coupling force $f_{b,i}$ in Eq. (2) is incorporated into the fluid momentum equations, and these are again advanced for several eddy turnover times, to achieve a new statistical stationary state. The statistical results are obtained at that point.

3.1 Bubble parameters

Before examining the turbulence modification, we briefly discuss the features of the simulations that incorporate two-way and one-way coupling. It should be noted that the parameter range that is manageable for simulations with momentum coupling is restricted, for justifying the applied point force approximation; in particular, this holds for active bubble-laden turbulent flows. As suggested by Boivin et al. [26] and Maxey and Riley [32], the fluid velocity u in Eq. (8) that is evaluated at the location of bubble *n* is required not to be disturbed by bubble *n*; at the same time it should include disturbances created by other bubbles. For the sake of computation, approximating velocity u by the one that is perturbed by all bubbles is necessary, which induces an error on the order of $O(a/h)$ [26].

On the other hand, as already emphasized by Mazzitelli et al. [5] and Van den Berg et al. [7], the non-uniform turbulence modification, namely enhancement of energy on small scales and reduction on large scales for two-way coupled bubble laden flows, is achievable when the bubble radius a is comparable to the Kolmogorov length scale of the flow: $a \cong \eta$. The bubble response time $\tau_b = 0.07\,\tau_\eta$ that is compatible with both the constraints $a \ll \Delta x$ and $a \cong \eta$ is thus chosen and fixed throughout all simulations. Here, a/η is ~0.6. The volume fraction V_f is 1.6 % (the number of bubbles is N_b = 161200) and various bubble regimes are examined by varying $\beta = (\langle u'^2 \rangle)^{1/2} / v_T$, which is a dimensionless parameter that quantifies the gravity force [5, 19]. The bubble regimes here correspond to micro-bubbles in clean water ($\nu = 10^{-6}$ m^{2}s^{-1}) with radii in the $a \sim$ 65-95 μm range. For simulations with one-way coupling, the coupling force in Eq. (2) is set to zero. Here, the number of bubbles is N_b = 50000 and the bubble response time is basically equal to that under the two-way coupling.

3.2 Turbulence modification

In the following Secs. 3.2.1 and 3.2.2, we explain in more detail the effects of two-way coupling on the flow velocity, flow vorticity, the flow dissipation spectrum, and the flow dissipation.

3.2.1 Modification of the fluid velocity

We first examine the effect of two-way coupling on the fluid velocity field. Shown in Table 1 is the root-mean squared fluid velocity fluctuation in the x_1, x_2, and x_3 directions, with respect to β. The plots show weaker velocity fluctuations in the vertical direction, compared with other directions, for all values of β, which is indicative of a reduction in the turbulence kinetic energy in this direction. To ascertain the mechanism that is responsible for this preferential attenuation, in the following section the fluid vorticity fields for the two-way coupling case will be analyzed. Here, a pair of two-way coupled fields (V_f = 1.6 %; β = 1.4) that are exactly the same are used. For one field, the coupling force $f_{b,i}$ in Eq. (2) is turned off. The advantages of this approach are two-fold: it not only enables a direct comparison between two vorticity fields that are initially the same, but also enables a more detailed analysis of the coupling force's influence on the evolution of vortical structures.

3.2.2 Modification of the fluid vorticity

Shown in Fig. 1 is the evolution of the vorticity component ω_2 in the x_1x_3 (xz) plane ($x_2 = \pi$), obtained at four successive time frames. It is seen that as the bubbles are attracted to the core of the vortical structures owing to the added mass force that is directed toward the regions of high vorticity, the magnitude of ω_2 increases more rapidly than for the one-way coupling case. It is also seen that once entrained, bubbles tend to accumulate in the downflow regions of the structures, owing to the lift force [5], and as the bubbles remain in the downflow regions, a faster reduction in the magnitude of ω_2 is detected. Now, we discuss the mechanisms for the enhancement and subsequent reduction of ω_2. It is obvious that bubbles that are attracted to the cores of the vortical structures agitate the local fluid velocity in their surroundings. Since the buoyancy term contributes strongly to the coupling force in Eq. (12), the portion of the structure swept by the bubbles will be significantly affected by the vertical component of the coupling force $f_{b,3}$ directed upward. This non-symmetry of the force exerted on

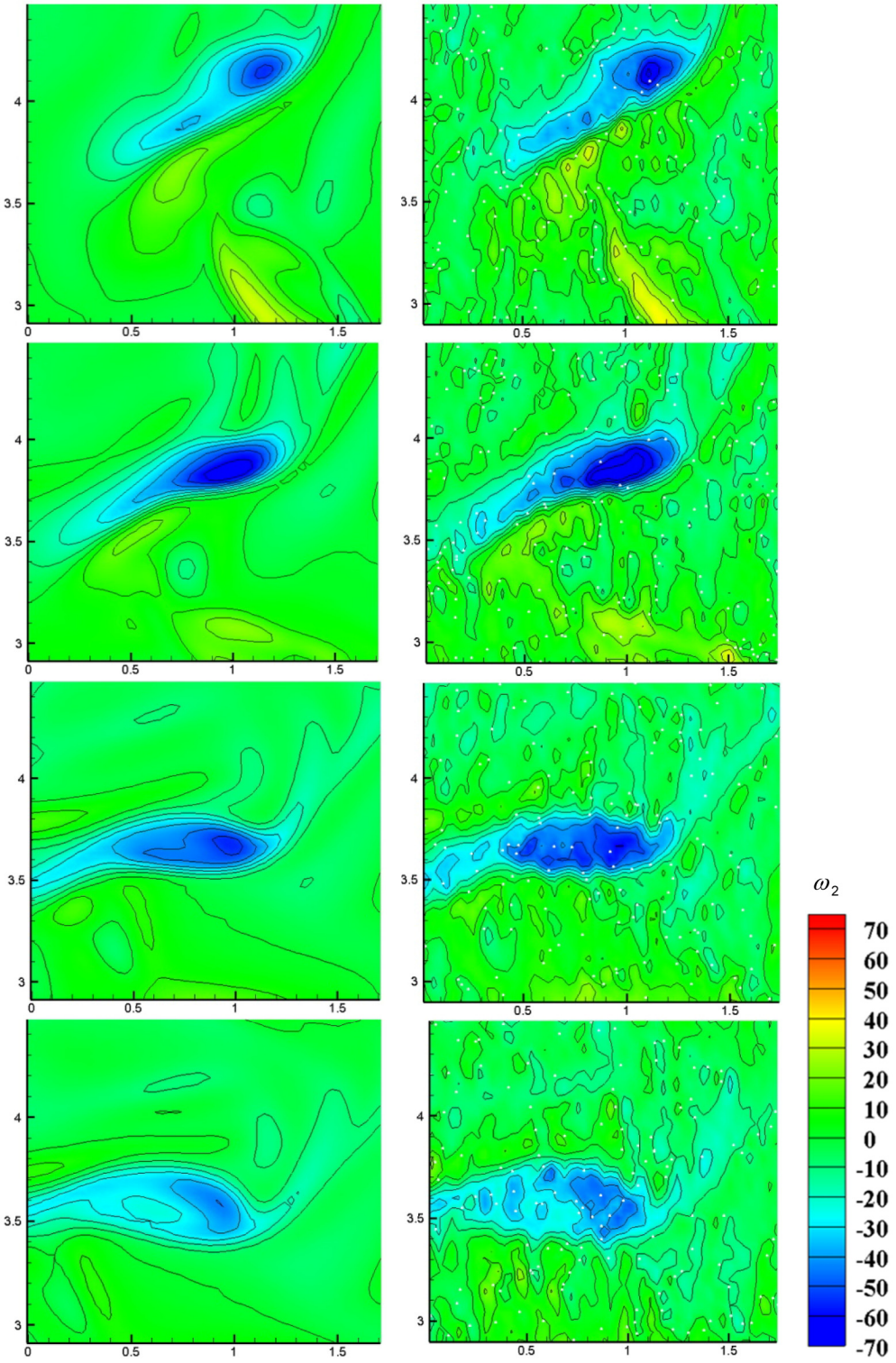

Fig. 1. Contours of the vorticity component ω_2 in the x_1x_3 (xz) plane for simulations with no coupling force (left column) and for simulations with two-way coupling force (right column, for $\beta = 1.4$ and $V_f = 1.6$ %) obtained at four successive time frames. The right panel of figures, from top to bottom, shows a sequence of interactions between negative (clockwise) vorticity (blue color) and bubbles (white dots). The time interval is ~1.5 τ_η .

the structure implies that local gradients of $f_{b,3}$ in the horizontal direction $\partial f_{b,3} / \partial x_1$ and $\partial f_{b,3} / \partial x_2$ can be created, increasing the magnitude of ω_2 . The fact that the generation of the gradients of $f_{b,3}$ induces a short-term increase in the magnitude of w_2 can also be clarified by examining the vorticity equations which are obtained by taking the curl of the fluid

Table 2. Volume fraction, root mean squared flow velocity fluctuation in the x_1, x_2, and x_3 directions, average flow enstrophy for two-way coupled simulations normalized by that of single-phase flows, average flow dissipation for two-way coupled simulations normalized by that of single-phase flows, average number of bubbles in the downflow regions normalized by total number of bubbles, bubble mean rising velocity compared with a quiescent fluid, and average enstrophy at the bubble location normalized by the average flow enstrophy with respect to β.

	V_f	$\langle u_1^2 \rangle^{1/2}_{2way}$	$\langle u_2^2 \rangle^{1/2}_{2way}$	$\langle u_3^2 \rangle^{1/2}_{2way}$	$\langle \Omega \rangle_{2way} / \langle \Omega \rangle_{1way}$	$\langle \varepsilon \rangle_{2way} / \langle \varepsilon \rangle_{1way}$	N_{down} / N_b	$(\langle v_z \rangle - v_T) / v_T$	$\langle \Omega \rangle_b / \langle \Omega \rangle$
$\beta = 2; v_T = 2v_\eta$	1.6 %	2.595	2.831	2.450	0.981	0.971	0.522(1way)	-0.123(1way)	1.401(1way)
							0.520	-0.091	1.388
$\beta = 1.4; v_T = 4v_\eta$	1.6 %	2.604	2.704	2.472	0.972	0.965	0.532(1way)	-0.097(1way)	1.330(1way)
							0.522	-0.056	1.278
$\beta = 0.7; v_T = 6v_\eta$	1.6 %	2.531	2.649	2.463	0.955	0.945	0.533(1way)	-0.076(1way)	1.202(1way)
							0.523	-0.034	1.176
$\beta = 1.4; v_T = 4v_\eta$	2.2 %	2.659	2.790	2.437	0.978	0.977	0.519	-0.045	1.261

momentum equations

$$\frac{D\omega_i}{Dt} = \omega_k \frac{\partial u_i}{\partial x_k} + \nu \frac{\partial^2 w_i}{\partial x_k \partial x_k} + \varepsilon_{ijk} \frac{\partial f_{b,k}}{\partial x_j}. \quad (16)$$

The above equation is rewritten for i = 2:

$$\frac{D\omega_2}{Dt} = \omega_k \frac{\partial u_2}{\partial x_k} + \nu \frac{\partial^2 \omega_2}{\partial x_k \partial x_k} - \frac{\partial f_{b,3}}{\partial x_1} + \frac{\partial f_{b,1}}{\partial x_3}, \quad (17)$$

confirming the enhancement of ω_2 by the creation of the gradients of $f_{b,3}$.

On the other hand, as the entrapment proceeds, bubbles trapped in the vortical structure tend to remain in the downflow regions of the structures, transferring the momentum to the fluid. Since the direction of the momentum transfer is essentially upward, the local fluid velocity in the downflow regions will be subjected to positive disturbances. This means that the magnitude of the vertical component of the fluid velocity U_3 in the downflow regions for two-way coupling is smaller than that for one-way coupling; hence, the magnitude of the gradients of U_3 in the horizontal directions $\partial U_3 / \partial x_1$ and. $\partial U_3 / \partial x_2$. Consequently, the magnitude of ω_2 is reduced. In addition, as the bubble clustering in the downflow regions continues, the cumulative effects of the bubbles overwhelm the previous increase in ω_2 by the local bubble forcing; thus, the vorticity decay is facilitated.

The vorticity decay caused by the attenuation of the local velocity gradients can also be understood by analyzing the mean rising velocity of bubbles and the number of bubbles in the downflow regions. As already emphasized by Aliseda and Lasheras [3] and Mazzitelli et al. [5], the reduction in the mean rising velocity is attributed to the increase in the bubble residence time in the downflow regions. However, owing to the collective effects of the interphase coupling in the downflow regions, the angular momentum in the vortical structures is reduced. Therefore, initially entrained bubbles are released out of the downflow regions faster than those in the one-way coupling case, leading to a slight reduction in the average number of bubbles in the downflow regions and accordingly enhancing their mean rising velocity, as shown in Table 2 and Fig. 2.

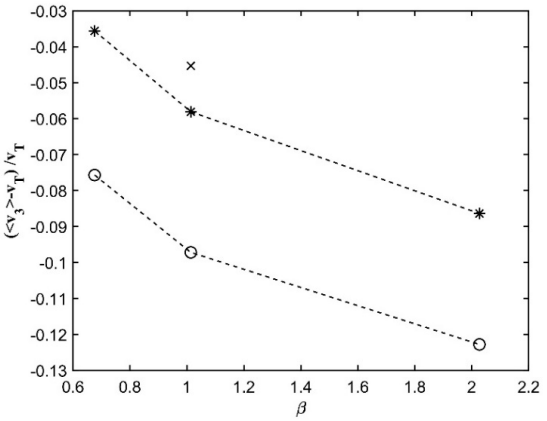

Fig. 2. Bubble mean rising velocity compared with a quiescent fluid, for simulations with one-way coupling (o), two-way coupling (*), and two-way coupling for V_f = 2.2 %(x) as a function of β.

A similar behavior was observed in the numerical simulations of a two-dimensional bubbly mixing layer, performed by Climent and Magnaudet [6]. They demonstrated that in their two-way coupling simulations, bubbles weakened the centripetal force contained in the vortex where they were trapped, by modifying the local fluid velocity gradient, substantially decreasing the interaction time with the structure.

We also examine how the accumulation of bubbles in the core of a vortical structure is influenced by the two-way coupling. Shown in Fig. 3 is the mean enstrophy at the bubble location, together with that for one-way coupling. The result indicates that the clustering of bubbles in the two-way coupling case becomes rather moderate compared with that in the one-way coupling case. As already pointed out by Mazzitelli et al. [5], the effect of active bubbles on the carrier flow is to decrease the fluid density, leading to a reduction in the effective fluid viscosity and hence turbulence kinetic energy. This indicates that bubbles in less dense flows are subjected to

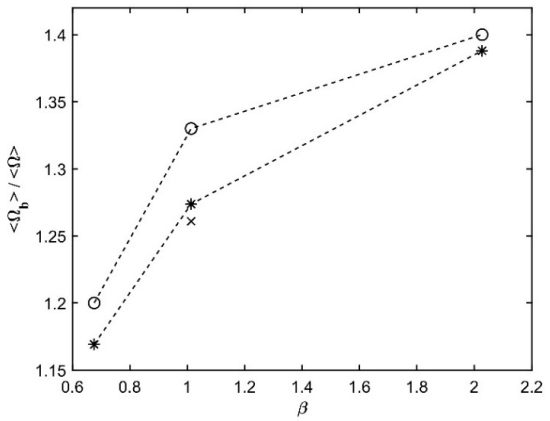

Fig. 3. Mean enstrophy at the bubble location normalized by the mean enstrophy of the fluid for simulations with one-way coupling (o), two-way coupling (*), and two-way coupling for V_f = 2.2 %(x) as a function of β.

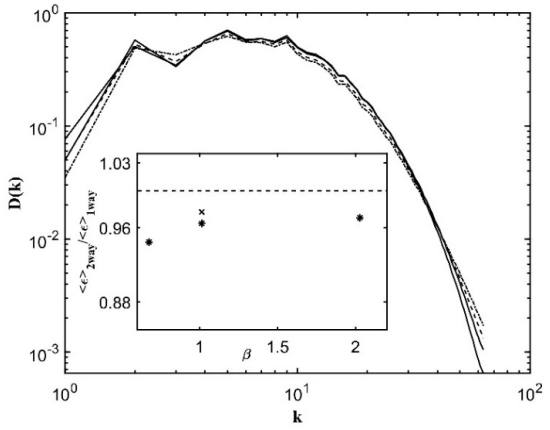

Fig. 4. Dissipation spectrum for the simulations with two-way coupling: $\beta = 2$, $v_T / v_\eta = 2$ (solid line), $\beta = 1.4$, $v_T / v_\eta = 4$ (dashed line), and $\beta = 0.7$, $v_T / v_\eta = 6$ (dotted-dashed line). The spectrum for the single-phase flow (thick solid curve) is plotted for comparison. The inset shows the average flow dissipation for simulations in the two-way coupling case, normalized by the single-phase flow result, as a function of β. The symbol x in the inset corresponds to V_f = 2.2 %.

stronger buoyancy forces than for the one-way coupling case, and this increase in the effective buoyancy force counteracts their clustering tendency.

3.2.3 Modification of the fluid dissipation spectrum

We now examine how the bubble-induced vorticity reduction affects the fluid dissipation spectrum and the average fluid dissipation. As already discussed above, local buoyancy forces transiently enhance the magnitude of ω_2, whereas the collective effect of the bubble cloud in the downflow regions is to suppress it. These two opposing effects appear to influence the transport of the fluid dissipation, which in turn links to the non-uniform distortion exhibited in the dissipation spectrum, shown in Fig. 4. In Fig. 4, the spectrum shows an increase in the energy at high wavenumbers (small scales), while the converse is observed at low wavenumbers (large scales), which is consistent with the findings of Mazzitelli et al. [5].

In addition, as the attenuation of the fluid vorticity owing to the cumulative momentum transfer dominates, the flow dissipation is reduced on average, compared with single-phase flows, as shown in the inset of Fig. 4. In Fig. 4, the maximal reduction occurs for $\beta = 0.7$, and the amount of the reduction decreases with increasing β. This trend can be explained as follows.

As already discussed extensively, the attenuation of the average fluid dissipation can be traced to the cumulative momentum transfer of bubbles located in the downflow regions of vortical structures. This implies that the amount of this attenuation is closely related not only to the number of bubbles in the downflow regions, but also to the rising velocity of bubbles v_T, since it dictates directly the intensity of the coupling force. In addition, the bubble rising velocity v_T is also related to the intensity of the bubbles' clustering in the downflow regions. As seen from Table 2, the ratio N_{down} / N_b increases with decreasing β. Mazzitelli and Lohse [4] also reported this phenomenon, and they attributed it to the lift force, because the magnitude of the lift force depends on the rising velocity v_T via $v-u$ comprising the lift force shown in Eq. (8), leading to the enhancement of clustering in the downflow regions with increasing rising velocity. Therefore, it can be concluded that the observed trend in β originates owing to the intrinsic behavior of bubbles within turbulence.

In the present simulations, the reduction in the dissipation was relatively small (on the order of 5 %), similar to the results reported by Mazzitelli et al. [5]. To demonstrate the origin of the weak modification, we tested another two-way coupling scenario by increasing the volume fraction V_f to 2.2 % (the number of bubbles was N_b = 241700) for $\beta = 1.4$. All the other parameters were the same. As seen from Table 2, the reduction in the dissipation for this scenario was smaller than for the previous case. Considering that increasing the volume fraction inevitably entails the energy increase caused by the local-bubble forcing, this observation implies that the large-scale energy attenuation in this case did not effectively balance out the energy enhancement on small scales. This implies that the more favorable condition for increasing the large-scale attenuation, rather than increasing the volume fraction, would be instead increasing the size of the bubbles, which risks violating the applied point-force approximation. In addition, the result again highlights the role of the bubbles' clustering in turbulence attenuation. As already discussed above, increasing the bubbles' radii (and therefore the bubbles' Stokes number) is strongly related to the enhanced clustering of bubbles in the downflow regions. This means not only that the bubbles' clustering plays a significant role in the turbulence modification, but also that the observed weak modification is a necessary consequence at least in the presently considered regime of micro-size bubbles.

The reason for this weak modification can also be highlighted by comparing the mechanism of the momentum transfer in bubble-laden turbulent flows and solid-particle laden flows with finite gravity. Solid particles with a small Stokes number

(τ_p / τ_η = 0.25, τ_p : particle response time) are likely to preferentially concentrate on the peripheries of vortical structures, where the local fluid velocity is directed downward [33, 34]. This indicates that the local fluid velocity on the side of the structures where the particles are swept experiences negative disturbances induced by the coupling force (drag force), leading to the enhancement of the vertical fluid velocity. Thus, together with the small-scale force that is also directed downward, the turbulence kinetic energy increases [34]. In contrast, bubbles, once caught in vortical structures, are apt to accumulate in the downflow regions and provide momentum in pursuit of smoothing the fluid velocity there. This offset in the downflow regions leads weakly alters the two-way coupled bubble-laden flow.

3.3 Bubble dispersion in the two-way coupling regime

In the previous section, we showed that two-way interactions affect the dynamics of vortical structures, leading to important alterations in the global properties of the carrier flow. Thus, we expect that this bubble-driven turbulence modification will affect the dispersion pattern of bubbles. To quantitatively explore such phenomena, several statistics such as the bubble Lagrangian velocity autocorrelation functions, the bubble diffusivity, and the pair dispersion were measured. These are presented in Secs. 3.3.1 and 3.3.2, respectively. In addition, statistics that were obtained for the one-way coupling scenario are presented as well, for highlighting the effects of the interphase coupling mechanism on the dispersion of bubbles. In addition, for each simulation, the corresponding statistics were obtained for different directions. The statistics in the horizontal (x_1 and x_2) and vertical (x_3) directions were computed separately, because in bubbly flows, the statistical properties in the vertical direction are different from those in the horizontal one, owing to buoyancy.

3.3.1 Bubble diffusivity

In this section, we first examine the bubble Lagrangian velocity autocorrelation functions. The Lagrangian velocity autocorrelation functions of bubbles and the bubble integral time-scale are defined according to

$$\rho_L^{b,i} = \frac{\left\langle v_i^b(x_0,t_0) v_i^b(x_0,t_0+t)\right\rangle}{\left\langle v_i^b(x_0,t_0)^2\right\rangle} \tag{18}$$

$$T_L^{b,i} = \int_0^\infty \rho_L^{b,i}(\mathrm{t})\mathrm{dt}, \tag{19}$$

where v_i^b denotes the bubble velocity fluctuation and the brackets denote ensemble averaging.

The bubble integral time scale is related to the bubble diffusivity as follows:

$$D_i^b = \left\langle (v_i^b)^2 \right\rangle T_L^{b,i} \tag{20}$$

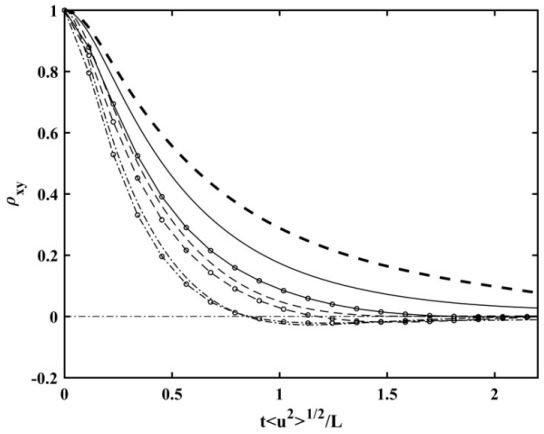

Fig. 5. Lagrangian velocity autocorrelation functions of bubbles in the horizontal direction, for simulations with one-way coupling (solid curve) and two-way coupling (○). The shown curves are for $\beta = 2$, $v_T / v_\eta = 2$ (solid curve), $\beta = 1.4$, $v_T / v_\eta = 4$ (dashed curve), and $\beta = 0.7$, $v_T / v_\eta = 6$ (dotted-dashed curve). The autocorrelation function of fluid particles (thick dashed curve) is shown as well.

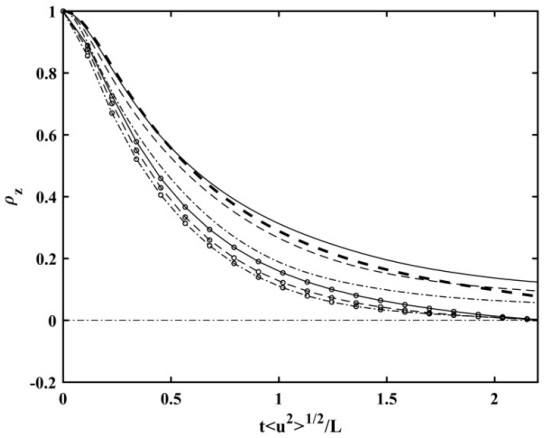

Fig. 6. Lagrangian velocity autocorrelation functions of bubbles in the vertical direction, for simulations with one-way coupling (solid curve) and two-way coupling (○). The shown curves are for $\beta = 2$, $v_T / v_\eta = 2$ (solid curve), $\beta = 1.4$, $v_T / v_\eta = 4$ (dashed curve), $\beta = 0.7$, $v_T / v_\eta = 6$ (dotted-dashed curve). The autocorrelation function of fluid particles (thick dashed curve) is shown as well.

In Fig. 5, the Lagrangian velocity autocorrelation functions of bubbles in the horizontal direction are plotted for the one-way coupling and two-way coupling simulations. For both cases, the decorrelation of the horizontal velocity at smaller β is noticeable. This suggests that as the rising velocity of the bubbles increases owing to the larger buoyancy effect, or with smaller β, the bubbles tend to escape more rapidly those regions in which their velocity retains its previous values, resulting in the smaller velocity correlation time [19]. In addition, the bubble Lagrangian velocity autocorrelation functions in the vertical direction for the one-way coupling and two-way coupling simulations are plotted in Fig. 6. The figure indicates that the vertical autocorrelation function decays faster with decreasing β, which is similar to the behaviors shown in the horizontal auto-

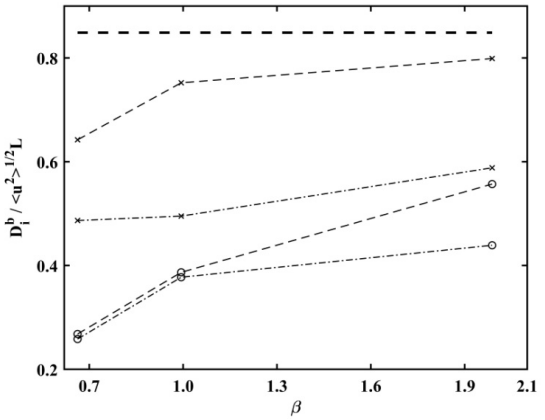

Fig. 7. Bubble diffusivity in the vertical (*) and horizontal (○) directions, for simulations with one-way coupling (dashed curve) and two-way coupling (dotted-dashed curve), together with the diffusivity of fluid particles (thick dashed curve) as a function of β .

correlation functions. In addition, compare with the horizontal autocorrelation, at β = 2 the correlation was stronger than that for the fluid particles. This suggests that bubbles lose the velocity correlation in the vertical direction slower than do the fluid particles, owing to their enhanced residence in the downflow regions, leading to this behavior [5, 19].

We now discuss the autocorrelation function behavior for two-way coupling simulation scenarios. As already discussed extensively in Sec. 3.2, in a turbulent bubbly flow where clustering at the center of a vortical structure takes place, the clustering is attenuated owing to the interphase coupling. Bubbles in the two-way coupling scenario rise rapidly compared with the one-way coupling scenario and for the same buoyancy effect, leading to the reduction in the velocity correlation time. Since $\left\langle (v_i^b)^2 \right\rangle$ in Eq. (20) does not depend on β, we expect that the difference can be better clarified by examining the bubble diffusivity. Shown in Fig. 7 is the bubble diffusivity as a function of β. The results confirm that the two-way coupling attenuates the bubble diffusivity, consistent with the conclusions of Mazzitelli and Lohse [19].

3.3.2 Pair dispersion

In the previous section, we examined the bubble diffusivity in the two-way coupling scenario. To gain further insights into the dependence of the bubble dispersion pattern on the interphase coupling mechanism, in this section we consider the pair dispersion of bubbles; namely, we investigate how the distance between a pair of bubbles depends on time. As has been already demonstrated both experimentally and numerically [35], the interphase momentum exchange affects the growth of the distance between a pair of bubbles. The pair dispersion for a pair of bubbles is defined according to

$$\left\langle \Delta X(t)^2 \right\rangle = \left\langle (X(t) - X(t_0))^2 \right\rangle, \tag{21}$$

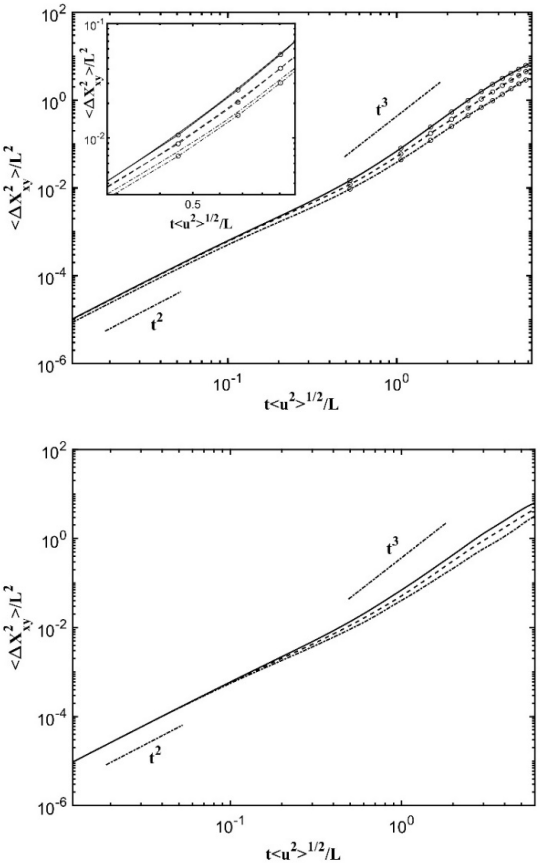

Fig. 8. Dispersion of bubble pairs in the horizontal direction, for simulations with one-way (top, no symbol) and two-way (bottom, ○) coupling. The curves shown in each figure are for $\beta = 2$, $v_T / v_\eta = 2$ (solid curve), $\beta = 1.4$, $v_T / v_\eta = 4$ (dashed curve), and $\beta = 0.7$, $v_T / v_\eta = 6$ (dotted-dashed curve). The inset shows a magnified view of the bubble pair dispersion in the horizontal direction, for simulations with one-way (no symbol) and two-way (○) coupling. The curves shown in the inset are for $\beta = 2$, $v_T / v_\eta = 2$ (solid curve), $\beta = 1.4$, $v_T / v_\eta = 4$ (dashed curve), and $\beta = 0.7$, $v_T / v_\eta = 6$ (dotted-dashed curve). The dispersion is calculated for bubble pairs with initial separation between 2η and 4η.

where $X(t)$ denotes the distance between a pair of bubbles, $X(t_0)$ is the initial separation, and the brackets denote averaging with respect to all bubble pairs.

First put forth by Richardson [36] and refined by Batchelor [37], the rate of the mean squared separation of pairs of the fluid particles with initial separation in the inertial subrange of turbulence is predicted to be quadratic in time ($\left\langle X(t)^2 \right\rangle \propto (\left\langle \varepsilon \right\rangle X(t_0))^{2/3} t^2$; the so-called Batchelor regime), followed by a transition to a super-diffusive regime where the separation scales cubically with t ($\left\langle X(t)^2 \right\rangle \propto \left\langle \varepsilon \right\rangle t^3$; the so-called Richardson regime), and ending with a linear increment of the separation at large times ($\left\langle X(t)^2 \right\rangle \propto T_L^{b,i} t$). The dispersion is calculated for pairs of bubbles that initially separate between 2 η and 4 η .

Fig. 8 shows the pair dispersion of bubbles in the horizontal

direction, for one-way and two-way coupling simulations. In the both cases, all dispersive regimes are observed, which is in agreement with the results reported by Mazzitelli and Lohse [19]. In addition, as the dispersion transitions into the Richardson regime, its dependence on β becomes pronounced. Similar trends were observed for the pair dispersion in the vertical direction (not shown). All of the scaling behaviors remain unchanged, and the β-dependence pertaining to the intensity of the growth of the separation is still noticeable.

This distinctive dependence on β can be explained as follows. As emphasized by Bourgoin [38] based on the work of Richardson [36], turbulence in the dispersion process, in particular uncorrelated motion owing to large-scale structures, is indispensable for ensuring the efficient separation of bubble pairs. This involvement that advocates the dispersion occurs in earnest when the pair separation extends beyond the dissipation subrange of the turbulence ($X(t) \ll \eta$). From that point and onward, structures with scale $X(t)$ become the most effective for the dispersion [39]. In addition, provided that their initial separation lies within the inertial subrange, the efficiency is manifested by the emergence of the Richardson scaling [35]. This suggests that as a pair of bubbles moves apart beyond the scale of the Batchelor regime and reaches a large-scale structure of scale $X(t)$ whose vertical velocity is on order of its rising velocity, turbulent motion can facilitate separation. In other words, as the value of β decreases, sufficient growth of the separation supported by the interactions with the structures becomes unlikely, since bubbles in this case tend to cross through the structure [5, 19]. This in turn decreases the growth of the separation.

Now, we discuss how the pair dispersion in the two-way coupling scenario differs from that in the one-way scenario. Since the momentum coupling between the two phases reduces the kinetic energy contained in the carrier turbulence, we expect that this reduction will manifest itself via the coefficient $\langle \varepsilon \rangle$, which characterizes the cubic growth in the Richardson regime. Indeed, as the transition toward the super-diffusive regime occurs, the smaller values of the mean squared separation are recognized for both the horizontal and vertical directions (not shown), compared with the one-way coupling scenario, as shown in the inset of Fig. 8. In addition, the amount of reduction becomes more noticeable for smaller β, revealing the β-dependence of the turbulence attenuation.

4. Conclusions

In this paper, we investigated the effects of two-way interactions, both on the isotropic turbulence and dispersion of bubbles, using direct numerical simulations. The trajectory of the bubbles was calculated using Lagrangian tracking, and the motion of the bubbles was assumed to be governed by added mass, gravity, drag, and lift force. The effects of the bubbles on the carrier flow were incorporated by applying the point-force approximation.

The attenuation of the vertical velocity fluctuations of the carrier flow was explained in terms of the vorticity fluctuations induced by the inclination of the local buoyancy forces to the upward direction, and by collective buoyancy effects in the downflow regions. This fluctuating behavior of vorticity affected the transport of the flow viscous dissipation with large-scale energy attenuation, compared with single-phase flows. The time-averaged result for this modulation revealed a reduction in the kinetic energy contained in the carrier flow. We also examined the dispersion statistics of the bubbles subjected to the interphase coupling effects. The dispersion still depended on the level of the buoyancy force. On the other hand, bubble-induced turbulence modification affected accumulation at the center of large-scale structures, yielding other factors that contributed to the bubble dispersion.

While the present work has provided detailed analysis of bubble dispersion in the two-way coupling scenario, there are some issues relevant to the bubble dispersion in the context of mutual interactions. As pointed out by Climent and Magnaudet [6], the two-way coupling effects on the carrier turbulence were significant when the accumulation of bubbles in vortical structures was distinctive. On the other hand, bubbles in the simulations that accounted for two-way coupling were found to leave their entrapped vortical structures more rapidly owing to the reduction in the fluid density [5, 6]. This suggests that the two-way coupling restricts significant modification of the carrier turbulence, which was already demonstrated in Sec. 3.2.2. This self-restraining effect suggests that dramatic modification of velocity and spatial distribution of bubbles is not available at least for the bubble regime considered in the present work. For bubbles beyond the present regime, the overall situation would be different.

Acknowledgments

We acknowledge the support by Samsung Science and Technology Foundation (Grant No. SSTF-BA1702-03).

References

[1] S. A. Thorpe, On the clouds of bubbles formed by breaking wind waves in deep water, and their role in air-sea gas transfer, *Philos. Trans. Roy. Soc. Lond.*, A304 (1982) 155-210.

[2] R. F. Mudde, Gravity-driven bubbly flows, *Ann. Rev. Fluid Mech.*, 37 (2005) 393-423.

[3] A. Aliseda and J. C. Lasheras, Preferential concentration and rising velocity reduction of bubbles immersed in a homogeneous and isotropic turbulent flow, *Phys. Fluids.,* 23 (9) (2011) 093301.

[4] I. M. Mazzitelli and D. Lohse, The effect of microbubbles on developed turbulence, *Phys. Fluids.*, 15 (1) (2003) L5-L8.

[5] I. M. Mazzitelli, D. Lohse and F. Toschi, On the relevance of the lift force in bubbly turbulence*, J. Fluid Mech.,* 488 (2003) 283-313.

[6] E. Climent and J. Magnaudet, Dynamics of a two-dimensional upflowing mixing layer seeded with bubbles: bubble dispersion and

effect of two-way coupling, *Phys. Fluids.,* 18 (10) (2006) 103304.
[7] T. H. Van den Berg, S. Luther and D. Lohse, Energy spectra in microbubbly turbulence, *Phys. Fluids*., 18 (3) (2006) 038103.
[8] D. Legendre and J. Magnaudet, The lift force on a spherical bubble in a viscous linear shear flow, *J. Fluid Mech.,* 368 (1998) 81-126.
[9] J. Magnaudet and I. Eames, The motion of high-Reynolds number bubbles in inhomogeneous flows, *Annu. Rev. Fluid Mech.,* 32 (2000) 659-708.
[10] D. Molin, C. Marchioli and A. Soldati, Turbulence modulation and microbubble dynamics in vertical channel flow, *Int. J. Multiphase Flows*., 42 (2012) 80-95.
[11] A. H. Abdelsamie and C. Lee, Decaying versus stationary turbulence in particle-laden isotropic turbulence: turbulence modulation mechanism, *Phys. Fluids*., 24 (2012) 015106.
[12] A. H. Abdelsamie and C. Lee, Decaying versus stationary turbulence in particle-laden isotropic turbulence: heavy particle statistics modifications, *Phys. Fluids*., 25 (2013) 033303.
[13] J. Lee and C. Lee, Modification of particle-laden near-wall turbulence: effect of Stokes number, *Phys. Fluids*., 27 (2015) 023303.
[14] J. Lee and C. Lee, The effect of wall-normal gravity on particle-laden near-wall turbulence, *J. Fluid Mech.,* 873 (2019) 475-507.
[15] B. Gereltbyamba and C. Lee, Flow modification by inertial particles in a differentially heated cubic cavity, *Int. J. Heat Fluid Flow*., 79 (2019) 108445.
[16] V. Eswaran and S. B. Pope, An examination of forcing in direct numerical simulations of turbulence, *Computers and Fluids.,* 16 (3) (1988) 257-278.
[17] P. K. Yeung and S. B. Pope, An algorithm for tracking fluid particles in numerical simulations of homogeneous turbulence, *J. Comput. Phys*., 79 (2) (1988) 373-416.
[18] P. D. M. Spelt and A. Biesheuvel, On the motion of gas bubbles in homogeneous isotropic flow, *J. Fluid Mech.,* 336 (1997) 221-244.
[19] I. M. Mazzitelli and D. Lohse, Lagrangian statistics for fluid particles and bubbles in turbulence, *New J. Phys.,* 6 (2004) 203.
[20] J. S. Hadamard, Mouvement permanent lent d'une sphere liquide et visqueuse dans un liquid visqueux, *C. R. Acad. Sci. Paris.,* 152 (1911) 1735-1738.
[21] W. Ribczynski, On the translating motion of a fluid sphere in a viscous medium, *Bull. Acad. Sci. Cracovie*., 40 (1911) 40-46.
[22] G. Shim, H. Park, S. Lee and C. Lee, Behavior of mi crobubbles in homogeneous stratified turbulence, *Phys. Rev. Fluids*., 5 (2020) 074302.
[23] I. Fouxon, G. Shim, S. Lee and C. Lee, Multifractality of fine bubbles in turbulence due to lift, *Phys. Rev. Fluids*., 3 (2018) 124305.
[24] J.-I. Choi, K. Yeo and C. Lee, Lagrangian statistics in turbulent channel flow, *Phys. Fluids.,* 16 (3) (2004) 779-793.
[25] P. G. Saffman, On the settling speed of free and fixed suspension, *Stud. Appl. Maths*., 52 (2) (1973) 115-127.
[26] M. Boivin, O. Simonin and K. D. Squires, Direct numerical simulation of turbulence modulation by particles in isotropic turbulence, *J. Fluid Mech*., 375 (1998) 235-263.
[27] M. R. Maxey, E. J. Chang and L. P. Wang, Simulation of interactions between microbubbles and turbulent flows, *Appl. Mech. Rev*. ,47 (6S) (1994) S70-S74.
[28] C. S. Peskin, Flow patterns around heart valves: a numerical method, *J. Comput. Phys.,* 10 (1972) 252-271.
[29] M. Uhlmann, An immersed boundary method with direct forcing for the simulation of particulate flows, *J. Comput. Phys.,* 209 (2005) 448-476.
[30] C. S. Peskin, The immersed boundary method, *Acta Numer.,* 11 (2002) 479-517.
[31] R. P. Beyer and R. J. Leveque, Analysis of a one-dimensional model for the immersed boundary method, *SIAM J. Numer. Anal.,* 29 (1992) 332-364.
[32] M. R. Maxey and J. Riley, Equation of motion for a small rigid sphere in a turbulent fluid flow, *Phys. Fluids.,* 26 (4) (1983) 883-889.
[33] L. P. Wang and M. R. Maxey, Settling velocity and concentration distribution of heavy particles in homogeneous and isotropic turbulence, *J. Fluid Mech*., 256 (1993) 27-68.
[34] A. Ferrante and S. Elghobashi, On the physical mechanisms of two-way coupling in particle-laden isotropic turbulence, *Phys. Fluids*., 15 (2) (2003) 315-329.
[35] J. T. Kim, J. Nam, S. Shen, C. Lee and L. P. Chamorro, On the dynamics of air bubbles in Rayleigh-Benard convection, *J. Fluid Mech.,* 891 (2020) A7.
[36] L. F. Richardson, Atmospheric diffusion shown on a distance-neighbor graph, *Proc. R. Soc. Lond. A,* 110 (1926) 709.
[37] G. K. Batchelor, The application of the similarity theory of turbulence to atmospheric diffusion, *Quart. F. R. Meteorol. Soc.,* 76 (328) (1950) 133-146.
[38] M. Bourgoin, Turbulent pair dispersion as a ballistic cascade phenomenology, *J. Fluid Mech*., 772 (2015) 678-704.
[39] S. Corrsin, Theories of turbulent dispersion, *Proc. Intern. Colloq. on Turbulence* (Marselle 1961), *Centr. Nat. Rech. Sci.* (1962) 27-52.

Hyoeun Shim is a graduate student of the School of Computational Science and Engineering, Yonsei University, Seoul, Korea. She received her master degree in Computational Science and Engineering from Yonsei University.

Changhoon Lee received his B.S. (1985) and M.S. (1987) from Seoul National University, Seoul, Korea and Ph.D. (1993) from UC Berkeley, USA in Mechanical Engineering. He is a Professor in the Department of Mechanical Engineering & School of Mathematics and Computing, Yonsei University, Korea. His research interests include fundamentals of turbulence, particle-turbulence interaction, numerical algorithms, air pollution modeling, stochastic processes and deep learning of turbulence.